Synchronize Inertial Readings From Multiple Mobile Devices in Spatial Dimension

Lei Xie, *Member, IEEE*, Qingliang Cai, *Student Member, IEEE*, Alex X. Liu, *Senior Member, IEEE*, Wei Wang, *Member, IEEE*, Yafeng Yin, *Member, IEEE*, and Sanglu Lu, *Member, IEEE*

***Abstract*— In this paper, we investigate the problem of space synchronization, i.e., *synchronizing inertial readings from multiple mobile devices in the spatial dimension*, in other words, multiple mobile devices are *space synchronized* to have the same 3-D coordinates except that each device is the origin of its corresponding coordinate. We propose a scheme called MObile Space Synchronization (MOSS) for devices with two sensors: an accelerometer and a gyroscope, which are available on most mobile devices. Accelerometer readings from multiple mobile devices on a human subject are used to *achieve* space synchronization when the human subject is moving forward, such as walking and running. Gyroscope readings from multiple mobile devices on a human subject are used to *maintain* space synchronization when the human subject stops moving forward, which means that we can no longer obtain the consistent acceleration caused by body moving forward. Experiment results show that our MOSS scheme can achieve an average angle deviation of 9.8° and an average measurement similarity of 97%.**

***Index Terms*— Space synchronization, mobile device.**

I. Introduction

A. Motivation

NOWADAYS, the mobile devices equipped with inertial sensors are widely used to perform motion sensing and human computer interaction [1]–[4]. For example, in virtual reality games, a moving human subject may be equipped with multiple mobile devices on different body parts (such as heads, arms, and legs) to capture the human's movement, as shown in Fig. 1(a) . In this case, it is very essential to fuse the readings from multiple mobile devices based on *synchronized coordinates*, so that they can be combined together to recover better orientation of the users' body parts and recognize the human activities.

In this paper, we investigate the problem of space synchronization, i.e., *synchronizing inertial readings from multiple mobile devices in the spatial dimension*, in other words, multiple mobile devices are *space synchronized* to have the same 3-D coordinates except that each device is the origin of its corresponding coordinate. A modern mobile device is often equipped with an Inertial Measurement Unit (IMU), which typically includes an accelerometer and a gyroscope, and sometimes a magnetometer as well for advanced models. The readings from IMU sensors are based on a local coordinate determined by the orientation of its body frame (or its mother board to be more precise). Fig. 1(b) shows the two local coordinates of a smartphone and a smartwatch, respectively, in solid arrows. For the multiple mobile devices placed at different body parts of a human subject, due to the different orientation of their body frames, their local coordinates are mostly likely different. Without space synchronization, the readings from the IMU sensors of different mobile devices are difficult to be correlated with each other. With space synchronization, these readings can be used jointly to better describe human movements. We call the synchronized coordinate of a device as its global coordinate. Fig. 1(a) and (b) shows the synchronized coordinates of the devices in dashed arrows. Space synchronization allows us to capture the movement of different body parts in the aligned 3-D coordinates, which helps to build more accurate 3-D models of human actions.

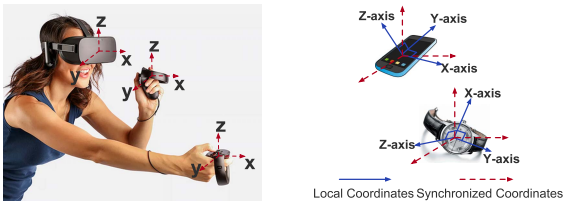

Fig. 1. Synchronize inertial readings from multi-devices in spatial dimension. (a) Synchronize 3-D coordinates among devices in VR games. (b) Local coordinates vs synchronized coordinates.

A straightforward solution to mobile device space synchronization is to use compasses or magnetometer sensors in mobile devices. Magnetometer readings allow each device to obtain the same magnetic field direction of the earth. Together with the same gravity direction of each device, all devices can therefore achieve space synchronization. This solution, although simple, have two weaknesses. First, most state-of-the-art wearable devices (such as Apple Watch S1, Samsung Watch Gear 2, and MOTO Watch 360) are not equipped with magnetometer sensors; in comparison, accelerometer and gyroscope sensors are available in most wearable devices. Second, magnetometer readings are often notoriously inaccurate in indoor environments [5], due to the magnetic interferences

Manuscript received October 29, 2017; revised May 10, 2018; accepted July 17, 2018; approved by IEEE/ACM TRANSACTIONS ON NETWORKING Editor K. Tang. Date of publication August 14, 2018; date of current version October 15, 2018. This work was supported in part by the National Natural Science Foundation of China under Grant 61472185, Grant 61472184, Grant 61321491, Grant 61502224, and Grant 61702257, in part by the Jiangsu Natural Science Foundation under Grant BK20151390 and Grant BK20170648, in part by the Fundamental Research Funds for the Central Universities under Grant 020214380035, in part by the National Science Foundation under Grant CNS-1421407, in part by the Jiangsu Innovation and Entrepreneurship (Shuangchuang) Program, and in part by the Collaborative Innovation Center of Novel Software Technology and Industrialization. *(Corresponding authors: Alex X. Liu; Sanglu Lu.)*

The authors are with the State Key Laboratory for Novel Software Technology, Nanjing University, Nanjing 210023, China (e-mail: lxie@nju.edu.cn; qingliangcai@dislab.nju.edu.cn; alexliu@nju.edu.cn; ww@nju.edu.cn; yafeng@nju.edu.cn; sanglu@nju.edu.cn).

Digital Object Identifier 10.1109/TNET.2018.2859246

caused by the massive steel embedded in building concrete structures and other metallic objects. Our empirical study further shows that the magnetometer readings are not reliable in typical indoor environment. Specifically, for different positions in the indoor environment, the angle deviation between the magnetometer measurement and the ground-truth north can be as large as 110°, the standard deviation of the magnetometer readings can be as large as 26.7°; for a fixed position in the indoor environment, with the interferences from different sources such as smart phone, earphone, metal plate, and magnet, the angle deviation between the magnetometer measurement and the ground-truth north can be as large as 133.6°, the standard deviation of the angle deviation can be as large as 86.3°.

B. Proposed Approach

In this paper, we propose a scheme called MObile Space Synchronization (MOSS) for devices with two sensors: an accelerometer and a gyroscope, which are available on most mobile devices. Accelerometer readings from multiple mobile devices on a human subject are used to *achieve* space synchronization when the human subject is moving forward, such as walking and running. Our insight on using accelerometer sensors to achieve space synchronization is that when the human subject moves forward, all attached mobile devices experience the same acceleration along the moving direction of the torso, which we call *consistent acceleration*. Although these mobile devices also experience various other accelerations due to intra-body movements (such as arm and leg movements), which we call *inconsistent acceleration*, they are usually much smaller than the *consistent acceleration* because intra-body movements are usually orders of magnitude smaller than the forward movement. When the human subject is moving forward, the approach of simply adding an inertial sensor on the human chest to directly measure the *consistent acceleration* seems to be a feasible solution, however, it cannot work effectively due to the following reasons: First, it still requires the other mobile devices to synchronize with this specified device in the spatial dimension, as the *consistent acceleration* can only be extracted directly from this device rather than all devices. Usually a magnetometer is essentially required for all devices to achieve this synchronization, however, this is contradictory to the situation we need to tackle. Second, even for this specified device, it may lead to inaccuracy in directly measuring the *consistent acceleration*, since the moving human body may usually introduce some *inconsistent accelerations*, more or less, into the measurements on the horizontal plane. Hence, in this paper, we choose to compute the forwarding direction by extracting the *consistent acceleration* from the accelerometer readings. We can treat the *inconsistent acceleration* as noises and use signal processing techniques to filter them out mostly. Moreover, using a low pass filter such as a Butterworth filter, the gravitational acceleration can be extracted from the acceleration measurements in the local coordinate system. Therefore, based on the forwarding direction and the gravitational direction as reference axes, the third axis can also be obtained since it is perpendicular to the plane defined by these two reference axes. Thus, according to these three axes, we can build the synchronized coordinates with each device as the origins.

Furthermore, we use gyroscope readings from multiple mobile devices on a human subject to *maintain* space synchronization when the human subject stops moving forward, which means that we can no longer obtain the consistent acceleration caused by forward body motion. After the human subject stops moving forward, his body parts may still slightly move or rotate. The gyroscope readings of a mobile device allow us to continuously track the small rotations along the three axes of the device's local coordinate. We derive a real-time rotation matrix corresponding to the orientation variation by integrating the rotation rates in different axes over time. Leveraging the stability of the gravity direction in the synchronized coordinates, we further calibrate the estimated rotation matrix from gyroscope tracking. Thus, we are able to *maintain* space synchronization even after the human subject stops moving.

C. Technical Challenges and Solutions

The first challenge is to extract the *consistent acceleration* of body movement when the human subject moves forward. This is challenging because both consistent and inconsistent accelerations are mixed together. As the mobile devices are attached to different body locations of the human subject, they perceive rather different accelerations in both the direction and magnitude during human motion. To address this challenge, we propose a principal component analysis (PCA) based scheme to remove the inconsistent accelerations from the observed accelerations. The key observation is that the consistent acceleration contributes to the observed accelerations of all mobile devices attached to the human subject. In other words, the observed acceleration signal of each device is the combination of the *consistent acceleration* signal, which is from the forwarding movement and the same for all devices, and the *inconsistent acceleration* signal, which is from the intra-body movement from and unique to the device itself. Furthermore, we observe that the inconsistent acceleration from the intra-body movement cancels each other out during the back and forth movement, and its expected value is close to 0 within a large enough time interval. Thus, the observed acceleration signals of multiple devices are strongly correlated, and therefore we can use PCA-based approach to cancel out the inconsistent factor and extract the consistent factor.

The second challenge is to address the accumulated errors in maintaining space synchronization when the human subject stops moving forward. It is well known that the errors in gyroscope based oriental tracking accumulate [6], [7]. Furthermore, the errors are further exacerbated by the large angular velocities and linear accelerations in human body motion. Current solutions primarily rely on Kalman filters; however, they only use a single data source from the gyroscope to calibrate the accumulated errors [8], which is not sufficient to further reduce the errors in maintaining space synchronization. To address this challenge, we propose a simple but effective complementary filter to calibrate the gyroscope tracking based on the stability of the gravity direction. We propose a rotation model that defines the rotations in the

orthogonal and parallel directions of the gravity, respectively. We then use this model to calibrate the gyroscope-based estimation with the Minimum Mean Square Error (MMSE) estimator.

D. Summary of Experimental Results

We implemented our MOSS system on mobile devices including Google Glass and Samsung S5 smart phones. They are deployed at different body locations of each human subject. We let the human subjects walk along different types of traces in outdoor environments with different moving modes, *i.e.*, walk, run, and jump. We use two main metrics to evaluate the performance: (1) *angle accuracy*: the angle deviation between the estimated human body movement direction and the ground truth, and (2) *coordinate accuracy*: the similarity between the synchronized coordinate and the ground truth. Experiment results show that MOSS achieves an average angle accuracy of 9.8° and an average coordinate accuracy of 97%. A real-world case study with free activities further shows that MOSS achieves an average angle accuracy of 12° and an average coordinate accuracy of 91%.

II. Related Work

Orientation Estimation: Much work has been done on estimating the orientation of a mobile device (such as a smartphone) using accelerometer, gyroscope, and magnetometer sensors [2], [6], [9]–[17]. Compared with our work, most of such work uses magnetometers. For example, Madgwick *et al.* [13] proposed a quaternion representation to incorporate accelerometer and magnetometer readings for orientation estimation . Zhou *et al.* [6] used the accelerometer and magnetometer to assist gyroscope in orientation estimation by selecting the best sensing capabilities. Gowda *et al.* [14] tried to map from a local frame of the sensor to a global frame of reference, so as to track a ball's 3D trajectory and spin with inertial sensors and radios embedded in the ball. Of prior work in this category, only two systems, Autowitness [18] and Nericell [19], which finds the rotation matrix between the local coordinate of a smartphone and the reference coordinate by the acceleration measurement, did not use magnetometers. They used a vehicle's forwarding accelerations (*i.e.*, speeding up and slowing down) obtained from accelerometer readings. Compared with our work, they have two key limitations as they attach mobile devices to moving vehicles rather than human subjects. First, as there is no intra-body movements and a vehicle moves much straighter than human moves, they do not need to deal with our first technical challenge. Second, as the mobile devices do not move after a vehicle stops, they do not need to deal with our second technical challenge.

Direction Estimation: Recently some work explored the estimation of heading directions for dead reckoning-based navigation schemes [20]–[26]. Compared with our work, most of such work uses magnetometers to estimate the heading directions while trying to mitigate the magnetic interference from indoor environments. For example, WalkCompass used magnetometers to estimate the walking direction of a human subject [20]. Walkie-Markie used the magnetometer and gyroscopes in smartphones to get the walking direction and turning angles of a human subject so that the indoor pathway maps can be obtained [21]. Wang *et al.* [22] used compasss, gyroscopes, and WiFi landmarks to estimate the absolute walking direction of a human subject. Of prior work in this category, only the APT system does not use magnetometer sensors [24]; instead, APT uses accelerometer and gyroscope sensors to obtain the walking direction of a human subject. Compared with our work, both the WalkCompass and APT does not address space synchronization among multiple mobile devices as they use only one smartphone. In contrast, in this paper we investigate multiple mobile devices instead of one device to synchronize the inertial readings from multiple devices in spatial dimension. We propose a more generalized solution to heading direction estimation for multiple wearable devices subject to different but correlated accelerations. Our solution neither relies on the inaccurate magnetometer measurements nor uses any application specific features.

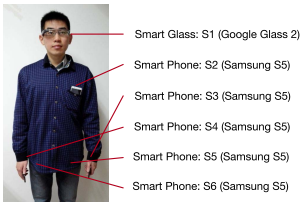

Fig. 2. Measurement setup.

III. Understanding Human Motions

A. Measurements

Measurement Setup: We placed six mobile devices, one smart glass (Google Glass 2) and five smartphones (Samsung Galaxy S5), at different body location of a human subject to continuously collect the inertial measurements in his daily life. As shown in Fig. 2, the Google Glass was placed on the head and the five phones were placed at five different locations on the body. These devices are all equipped with an accelerometer, a gyroscope, and a magnetometer. We use the three axes obtained from the magnetometers as the reference global coordinate.

Measurement of Human Body Movements: We observed that when the human subject attached with multiple mobile devices moves forward, the inconsistent accelerations from intra-body movement have different directions and magnitude. To extract the consistent and the inconsistent accelerations, we let the human subject walk along a straight path for 30 seconds. We attached an additional IMU sensor on the chest to estimate the ground-truth of the consistent acceleration as the inconsistent accelerations on the chest is negligible. We collected the acceleration measurements from the six devices as mixed accelerations and then extract the inconsistent accelerations from each device by subtracting the consistent acceleration. To illustrate the direction and magnitude of both the consistent and inconsistent accelerations, we plot them as vectors in the polar coordinate system corresponding to the earth coordinate system. We plot a vector of the inconsistent acceleration for every 100 ms during the time interval of 5 seconds. Fig. 3 shows the directions and magnitudes of the original

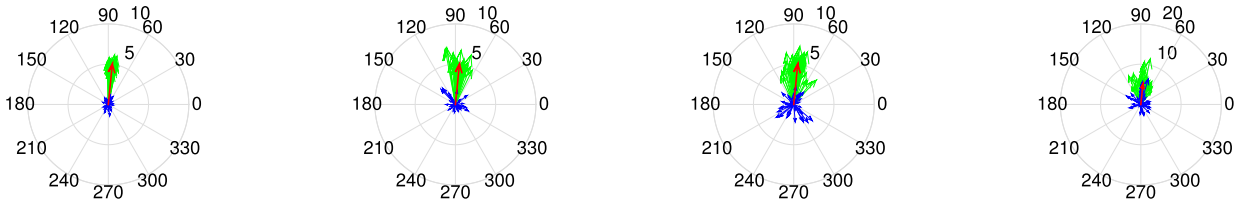

Fig. 3. The directions (°) and magnitudes (m/s^2) of the original/consistent/inconsistent accelerations in different devices. (a) S_1. (b) S_2. (c) S_3. (d) S_6.

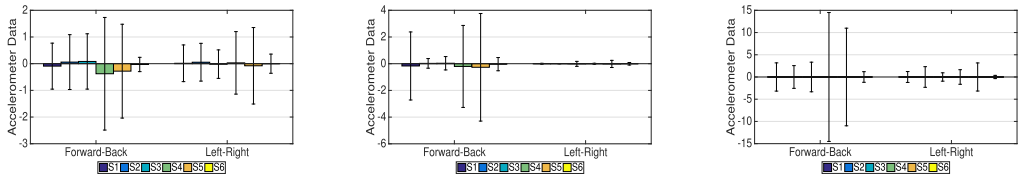

Fig. 4. The mean and standard deviation of different accelerations. (a) The mixed accelerations (m/s^2). (b) The consistent accelerations (m/s^2). (c) The inconsistent accelerations (m/s^2).

accelerations, the consistent accelerations, and the inconsistent accelerations, respectively, with the color green, red and blue. Without loss of generality, we plot these accelerations in the polar system for the devices S_1, S_2, S_3 and S_6. We observed that, for the inconsistent accelerations, the average magnitudes of the inconsistent accelerations are different among different devices, because they depend on the motion amplitudes in different body parts. Moreover, the directions of the inconsistent accelerations are distributed by and large evenly on the horizontal plane, because the accelerations of intra-body movements often mutually offset each other in opposite directions due to back and forth body part movement such as arm swing.

We observed that the mean value of inconsistent accelerations is close to 0 in each direction for a sufficiently large time window (such as 10 seconds), although the standard deviations of inconsistent accelerations are fairly large. Fig. 4 shows the mean and standard deviation of the mixed, consistent, and inconsistent accelerations, respectively, in the forward-back direction and the left-right direction of human motions. We observed that although the standard deviations of all accelerations are fairly large, their mean values are all relatively small. In regard to the inconsistent accelerations, for both directions, the standard deviations are usually in the order of $1m/s^2$. The standard deviations in the forward-back direction are significantly greater than the left-right direction, due to the reason that the human subject is moving forward. However, for both directions, the mean values of the inconsistent accelerations are all in the order of $10^{-5}m/s^2$. This implies that, although the inconsistent accelerations have different directions and magnitudes, the overall impact of the inconsistent accelerations from the intra-body movement can be negligible statistically.

B. Modeling of Human Motions

Let $\mathbf{f}_i(t)$ denote the mixed acceleration measured from device D_i at time t. Here $\mathbf{f}_i(t)$ consists of consistent acceleration $\mathbf{f}_c(t)$ and inconsistent acceleration $\mathbf{f}'_i(t)$, *i.e.*, $\mathbf{f}_i(t) = \mathbf{f}_c(t) + \mathbf{f}'_i(t)$. The accelerations are originally measured according to the local coordinate system of the device. As the human subject is moving, the local coordinate system is rotating over time relative to the earth coordinate system; thus, the acceleration measurements cannot describe human motions consistently. Suppose we can build a fixed coordinate system relative to the earth coordinate system. For the fixed coordinate system, we use $f_{i,x}(t), f_{i,y}(t)$, and $f_{i,z}(t)$ to denote the projections of $\mathbf{f}_i(t)$ in x, y and z axes, respectively, and use $f'_{i,x}(t), f'_{i,y}(t)$, and $f'_{i,z}(t)$ to denote the projections of $\mathbf{f}'_i(t)$ in x, y, and z axes, respectively. Let the angles between $\mathbf{f}_c(t)$ and each x, y and z axis at time t be $\alpha_i(t)$, $\beta_i(t)$, and $\gamma_i(t)$, respectively. Since the consistent acceleration $\mathbf{f}_c(t)$ has a fixed direction with respect to the coordinate system, $\alpha_i(t)$, $\beta_i(t)$, and $\gamma_i(t)$ are all constant values over time; thus, we denote them as α_i, β_i, and γ_i, respectively, for simplicity. Thus, the direction of $\mathbf{f}_c(t)$ can be represented as a unit vector $\langle \cos\alpha_i, \cos\beta_i, \cos\gamma_i \rangle$. Let $f_c(t)$ denote the magnitude of the consistent acceleration in the forwarding direction; thus, its projection on the x, y and z axes are $f_c(t)\cos\alpha_i$, $f_c(t)\cos\beta_i$, and $f_c(t)\cos\gamma_i$, respectively. The projections on the three axes are as follows:

$$\begin{cases} f_{i,x}(t) = f_c(t)\cos\alpha_i + f'_{i,x}(t), \\ f_{i,y}(t) = f_c(t)\cos\beta_i + f'_{i,y}(t), \\ f_{i,z}(t) = f_c(t)\cos\gamma_i + f'_{i,z}(t). \end{cases} \tag{1}$$

Fig.5 shows the relationship among $\mathbf{f}_i(t)$, $\mathbf{f}_c(t)$, and $\mathbf{f}'_i(t)$, as well as the projection of $\mathbf{f}_c(t)$ on the three axes.

Thus, if we can compute the value of $\cos\alpha_i, \cos\beta_i$, and $\cos\gamma_i$, we can calculate the direction of the consistent acceleration $\mathbf{f}_c(t)$ in the corresponding coordinate system. Further, for any inconsistent accelerations corresponding to the intra-body movement, we observe that the mean value of the inconsistent accelerations is close to 0, as long as the time interval is large enough. The following theorem captures the above characteristics:

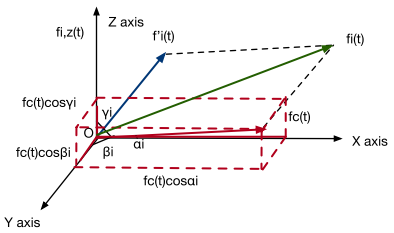

Fig. 5. $\mathbf{f}_i(t)$ consists of consistent acceleration $\mathbf{f}_c(t)$ and inconsistent acceleration $\mathbf{f}'_i(t)$, the projection of $\mathbf{f}_c(t)$ on the x, y and z axes are $f_c(t)\cos\alpha_i$, $f_c(t)\cos\beta_i$, and $f_c(t)\cos\gamma_i$, respectively.

Theorem 1: For a fixed coordinate system relative to the earth coordinate system, for any inconsistent acceleration $\mathbf{f}'_i(t)$ caused by intra-body movements, the expected value of $\mathbf{f}'_i(t)$ is approximately equal to 0 within a sufficiently large time interval $[t_s, t_e]$. That is,

$$E[\mathbf{f'}_i(t)] = \frac{1}{t_e - t_s}\int_{t_s}^{t_e} \mathbf{f}'_i(t)dt \approx 0. \tag{2}$$

Proof: Without loss of generality, we prove this theorem for x-axis. Our reasoning is applicable for other axes. Let $\Delta v_{i,x}$ denote the change of the relative velocity between device D_i and the body after the intra-body movements occurred during time interval $[t_s, t_e]$. According to the relation between velocity and acceleration, we have $\Delta v_{i,x} = \int_{t_s}^{t_e} f'_{i,x}(t)dt$. As body parts move back and forth, the amplitudes of the intra-body movement are usually small and do not change significantly in any direction. Thus, $\Delta v_{i,x}$ should be smaller than a constant threshold C. In general situations, $C \leq 0.4$m/s due to the back-and-forth moving property.

Thus, let $\Delta t = t_e - t_s$, for $E[f'_{i,x}(t)]$, *i.e.*, the expected value of the acceleration $f'_{i,x}(t)$ during $[t_s, t_e]$, we have

$$E[f'_{i,x}(t)] = \frac{1}{\Delta t}\int_{t_s}^{t_e} f'_{i,x}(t)dt = \frac{\Delta v_{i,x}}{\Delta t} < \frac{C}{\Delta t}. \tag{3}$$

If the time interval $\Delta t = t_e - t_s$ is sufficiently larger than the value of C, then $E[f'_{i,x}(t)] \approx 0$, e.g., $\Delta t = 20$s and $C = 0.4$m/s, $\Delta t \gg C$, then $E[f'_{i,x}(t)] \leq \frac{0.4}{20}\text{m/s}^2 = 2 \times 10^{-2}\text{m/s}^2 \approx 0$. □

Theorem 1 implies that, during a sufficiently large time interval, *e.g.*, 10∼20s, the expected value of the inconsistent acceleration can be negligible, as the inconsistent accelerations cancel each other out during the back and forth movements. This explains our observations that the mean value of the inconsistent acceleration is in the order of 10^{-5}m/s^2.

IV. Space Synchronization Model

A. Achieve Space Synchronization

The objective of space synchronization for mobile devices is to align their local coordinate to their global coordinate. We use the direction cosine representation to quantify the orientation difference between the local and global coordinates of each device. In the direction cosine representation, the orientation of the local coordinate relative to the global coordinate system is specified by a 3×3 rotation matrix $\mathbf{C}$, where each column is a unit vector along one axis in the local coordinate specified in terms of the global coordinate axes.

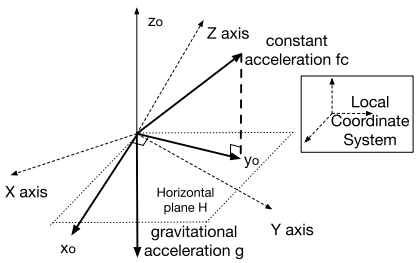

Fig. 6. Deriving the global coordinate.

A vector quantity v_l defined in the local coordinate system is equivalent to the vector $v_g = \mathbf{C} \cdot v_l$ defined in the global coordinate. The inverse transformation is $v_l = \mathbf{C}^T \cdot v_g$ as the inverse of a rotation matrix is equal to its transpose.

For the local coordinate of a device, assuming that we can extract a constant acceleration as a vector $\mathbf{f}_c$ from the acceleration measurements and extract a constant gravitational acceleration as a vector $\mathbf{g}$ from the low pass filter (such as the Butterworth filter [27]), we can build the global coordinate and compute the rotation matrix as follows. After we obtain the gravity vector $\mathbf{g}$, we derive its opposite value and normalize this vector as $\mathbf{z}_o = \frac{-\mathbf{g}}{\|\mathbf{g}\|}$, we then set this vector to represent the global Z-axis as it is in the opposite direction of the gravitational acceleration. We set the vector $\mathbf{z}_o$ to represent to be perpendicular to the horizontal plane. After computing the cross product $\mathbf{y} = \mathbf{g} \times \mathbf{f}_c$, we obtain a vector $\mathbf{y}$ that is perpendicular to the plane determined by the two distinct but intersecting lines corresponding to $\mathbf{g}$ and $\mathbf{f}_c$. We normalize this vector as $\mathbf{y}_o = \frac{\mathbf{y}}{\|\mathbf{y}\|}$. Since the vector $\mathbf{y}_o$ is on the horizontal plane, we set this vector to represent the global Y-axis. After that, by computing the cross product $\mathbf{x} = \mathbf{g} \times \mathbf{y}$, we obtain a vector $\mathbf{x}$ that is orthogonal to the plane determined by the two distinct but intersecting lines corresponding to $\mathbf{g}$ and $\mathbf{y}$. We normalize this vector as $\mathbf{x}_o = \frac{\mathbf{x}}{\|\mathbf{x}\|}$. Since the vector $\mathbf{x}_o$ is on the horizontal plane, and it is orthogonal to the global Y-axis and Z-axis, we set it to represent the global X-axis. After we obtain the vectors $\mathbf{x}_o$, $\mathbf{y}_o$, and $\mathbf{z}_o$ in the local coordinate, which correspond to the global X, Y, and Z-axes, we can derive the rotation matrix $\mathbf{C}^T$. Fig. 6 illustrates the above process.

B. Maintain Space Synchronization

As the orientation of a device may be continuously changing, we need to track and update the rotation matrix $\mathbf{C}$ over time. For example, if the rotation matrix at time t is given by $\mathbf{C}_t$, then the rotation matrix $\mathbf{C}_{t+\delta t}$ at time $t + \delta t$ can be computed as the product of two matrices

$$\mathbf{C}_{t+\delta t} = \mathbf{C}_t \mathbf{A}_{t,t+\delta t} \tag{4}$$

where $\mathbf{A}_{t,t+\delta t}$ is the rotation matrix relating the local coordinate at time t to the one at time $t+\delta t$. To estimate the matrix $\mathbf{A}_{t,t+\delta t}$, we use gyroscope measurements. According to the small angle approximation [12], if we use $\omega_x(t)$, $\omega_y(t)$, and $\omega_z(t)$ to represent the rotation rate of small rotations about its x, y and z axes between time t and $t + \delta t$, then

$$\mathbf{A}_{t,t+\delta t} = \exp\left(\int_t^{t+\delta t} \Omega(t)dt\right) \tag{5}$$

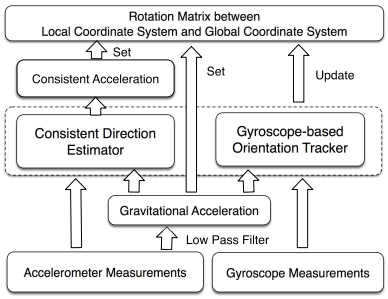

Fig. 7. System architecture.

where

$$\Omega(t) = \begin{bmatrix} 0 & -\omega_z(t) & \omega_y(t) \\ \omega_z(t) & 0 & -\omega_x(t) \\ -\omega_y(t) & \omega_x(t) & 0 \end{bmatrix} \tag{6}$$

We further use Taylor expansion of the exponential term to approximate the value of $\exp(\int_t^{t+\delta t} \Omega(t)dt)$.

As the angular velocity signals obtained from the gyroscopes are "integrated" to track and update the rotation matrix, the errors in the gyroscope signals propagate into the calculated orientation leading to large cumulative tracking errors. The tracking errors in the rotation matrix $\mathbf{A}_{t,t+\delta t}$ are amplified in each axis through the exponential function in Eq.(5). The larger the angular velocities and linear accelerations in the forward moving direction are, the more the tracking errors $e_x(t)$, $e_y(t)$, and $e_z(t)$ in that direction. Thus, the rotation matrix $\widehat{\mathbf{A}}_{t,t+\delta t}$ derived from gyroscope tracking is prone to large accumulation of errors after long periods. It is essential to leverage other measurements (such as the accelerometer measurements) for further calibration.

V. System Overview

The system architecture is shown in Fig. 7. MOSS consists of two components: a *Consistent Direction Estimator* for achieving space synchronization, and a *Gyroscope-based Orientation Tracker* for maintaining space synchronization. *Consistent Direction Estimator* uses principal component analysis to extract the magnitude of consistent acceleration from multiple devices, and further estimate the direction of consistent acceleration. Combined with the gravity direction extracted from the acceleration measurements, it generates a rotation matrix for space synchronization. *Gyroscope-based Orientation Tracker* continuously estimates the orientation variation of the body frame from the gyroscope measurements. Leveraging the stability of the gravitational accelerations in the global coordinate, we calibrate the rotation matrix using the Minimum Mean Square Error (MMSE) estimator.

To perform space synchronization among multiple devices, MOSS uses a server to communicate with these devices and process the corresponding measurements. We can set one of the mobile devices such as a smart phone as the server, as long as it can communicate with the other devices via wireless connections, and it has enough computing power for signal processing. MOSS consists of the following four steps.

(1) *Beacon Broadcasting:* The server first broadcasts a synchronization beacon to all devices. All devices start to record the accelerometer and gyroscope measurements after receiving this beacon. Let this time be t_0.

(2) *Local Measurement with Gyroscope Tracking:* For each time t within a time window W, each device D_i extracts the gravitational acceleration $\mathbf{g}_i(t)$ and the linear acceleration $\mathbf{f}_i(t)$ from the acceleration measurements in its local coordinate. Meanwhile, each device D_i tracks the rotation speed $\omega_i(t)$ in each axis from the gyroscope, and computes the rotation matrix $\mathbf{A}^i_{t_0,t}$ from time t_0 to t. After time window W, device D_i sends the following to the server: the rotation matrix $\mathbf{A}^i_{t_0,t}$, the gravity $\mathbf{g}_i(t)$, and the linear acceleration $\mathbf{f}_i(t)$ for all $t \in W$.

(3) *PCA Analysis:* After receiving the responses from all devices, the server performs PCA to extract the magnitude and estimates the direction of the consistent acceleration $\mathbf{f}_c(t)$ in the local coordinate of each device. With the gravity direction, it constructs a rotation matrix $\mathbf{C}^i_{t_0}$ for each device at time t_0, and sends $\mathbf{C}^i_{t_0}$ to each device.

(4) *Local Rotation Update:* Each device D_i locally updates the rotation matrix $\mathbf{C}^i_t$ using the matrix $\mathbf{A}^i_{t_0,t}$ from gyroscope tracking, *i.e.*, $\mathbf{C}^i_t = \mathbf{C}^i_{t_0}\mathbf{A}^i_{t_0,t}$. It then transforms the accelerometer and gyroscope measurements from the local coordinate to global coordinate.

VI. Consistent Acceleration Extraction

As the accelerometer measurements from multi-devices are highly correlated, we perform Principal Component Analysis (PCA) to extract the consistent acceleration during the process of moving forward. This consists of three steps: preprocessing, principal component extraction, and direction estimation.

A. Preprocessing

Suppose the acceleration measurements $\mathbf{f}_i(t)$ for each device D_i can be obtained as $\langle x_i(t), y_i(t), z_i(t)\rangle$ from the x, y, and z-axes in its local coordinate $L_i(t)$ at time t. Then, we can use the rotation matrix $(\mathbf{A}^i_{t_0,t})^T$ to transform the acceleration measurements from the current local coordinate $L_i(t)$ at time t to the reference local coordinate $L_i(t_0)$ at time t_0, *i.e.*,

$$\begin{bmatrix} x_i(t_0) \\ y_i(t_0) \\ z_i(t_0) \end{bmatrix} = (\mathbf{A}^i_{t_0,t})^T \begin{bmatrix} x_i(t) \\ y_i(t) \\ z_i(t) \end{bmatrix} \tag{7}$$

Thus, we obtain the acceleration measurements in the *reference local coordinate*, *i.e.*, the local coordinate at time t_0, which is therefore consistent over time.

Further, as we focus on extracting the forwarding accelerations on the horizontal plane, to avoid the interferences such as the up-and-down accelerations from the vertical direction during human motions, we project the linear acceleration $\mathbf{f}_i(t)$ onto the horizontal plane in the reference local coordinate system, as shown in Fig. 8.

B. Principal Component Extraction

The acceleration measurements of different axes on multiple devices are highly correlated, as shown in Eq.(1), because of the consistent acceleration $f_c(t)$. This can be observed

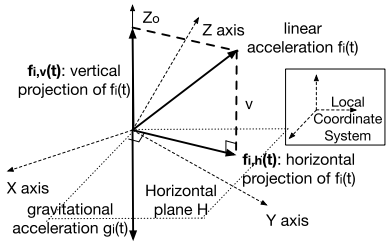

Fig. 8. Project acceleration $\mathbf{f}_i(t)$ onto horizontal plane.

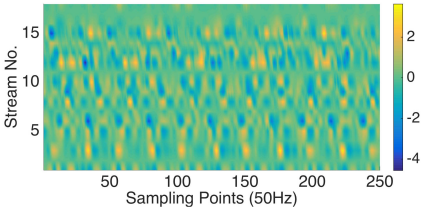

Fig. 9. Correlations among 18 streams of acceleration measurements from 6 devices in 3 axes.

from Fig. 9, which plots the 18 streams of acceleration measurements from 6 devices in 3 axes within a time interval of 5 seconds. Thus, to effectively extract the consistent acceleration $f_c(t)$, we apply PCA to discover the correlation among the streams of acceleration measurements. With PCA, we can track the time-varying correlations among the streams of acceleration measurements, and extract the principal components of these streams. This includes the following three steps.

(1) *Preprocessing:* Suppose the number of devices is m, we organize the data set as a matrix X consisting of p streams of acceleration measurements in 3 axes of local coordinate from m devices, where $p = 3 \times m$. Each column of the matrix X corresponds to one stream of acceleration measurements within a sampling window of size n. We choose the default time interval of the sampling window to be 10 seconds as the sampling process should not be too long for human motions and meanwhile the number of samples is large enough to ensure accurate correlation estimation. Therefore, the matrix X is of dimensions $n \times p$. Our solution first calculates the empirical mean μ_i along each column of the data matrix X, and then subtracts the empirical mean vector μ_i from each column ($i = 1 \cdots p$).

(2) *Covariance Estimation:* We calculate the covariance matrix as $X^T \times X$. The covariance matrix has the dimension of $p \times p$, where p is the number of streams for acceleration measurements. Then, we obtain the eigenvectors and eigenvalues of the covariance matrix, and construct the principal components using the equation $x_j = X \times q_j$, where q_j and x_j are the jth eigenvector and the jth principal components, respectively.

(3) *Consistent Forwarding Acceleration Extraction:* We select the first principal component x_1 to estimate the magnitude of the consistent acceleration. We further plot the PCA results in Fig. 10 to compare with the ground truth of consistent acceleration. According to the experiment results, the correlation between the PCA result and the ground truth is up to 0.961, which implies that we can accurately extract the consistent acceleration using PCA.

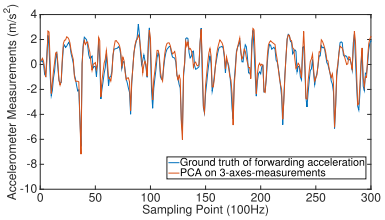

Fig. 10. PCA result vs. ground truth.

C. Direction Estimation

After principal component extraction, we obtain the magnitude of the *consistent acceleration* $\mathbf{f}_c(t)$, as shown in Fig. 10. It is known that $\mathbf{f}_c(t)$ has a fixed direction, *i.e.*, the forwarding direction, in regard to the *reference local coordinate*. During the process of human body movements, the magnitude of $\mathbf{f}_c(t)$, *i.e.*, $f_c(t)$, keeps changing along or against the fixed direction. Hence, if we specify the magnitude $f_c(t)$ along the fixed direction as positive value, then the magnitude $f_c(t)$ against the fixed direction can be specified as negative value. Next, for each device D_i, we need to further estimate the direction of $\mathbf{f}_c(t)$ in its local coordinate.

According to Theorem 1, the expected value of the *inconsistent acceleration* from intra-body movement, *i.e.*, $f_i'(t)$, is approximately equal to 0 in a sufficient large time interval. It can be regarded as "white noises" in comparison to the consistent acceleration from the forwarding movement, since the former is usually orders of magnitude smaller than the latter. Hence, in order to extract the components of *consistent acceleration* in various axes, while eliminating the interference from the *inconsistent acceleration*, we can select a sufficiently large time interval, add up the acceleration measurements for each axis according to Eq.(1), and obtain the estimate of each component in the corresponding axis. However, we need to tackle the following issue: As shown in Fig. 10, while the human subject is moving forward, the *consistent acceleration* $\mathbf{f}_c(t)$ keeps changing around the zero point even during one stride. Nevertheless, on the macro level, the moving speed of human subject usually keeps constant or does not change too much. This implies that the expected value of $f_c(t)$ should also be close to 0 (it is in the order of $10^{-3} \sim 10^{-2}$ m/s^2 according to the empirical study), when a human subject is moving in almost constant speed. In this regard, even if the *consistent acceleration* $\mathbf{f}_c(t)$ has a much larger magnitude than the *inconsistent acceleration* $\mathbf{f}_i'(t)$, when we add up the *consistent accelerations*, the positive and negative components cancel each other to approach a rather small value, which prevents us to distinguish the *consistent accelerations* from *inconsistent accelerations*.

Fortunately, since we can obtain the magnitude of $\mathbf{f}_c(t)$, *i.e.*, $f_c(t)$, via principal component extraction, by using the techniques such as linear interpolation, we can identify the time intervals where the value of $f_c(t)$ is positive, we call these time intervals *positive time intervals*. Similarly, we can also identify the *negative time intervals* where the value of $f_c(t)$ is negative. Fig. 11 shows an example of identifying the positive time interval according to the PCA results. Then, for each axis, without loss of generality, we can add up

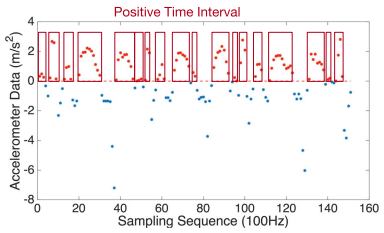

Fig. 11. Identify the positive time interval according to the PCA results.

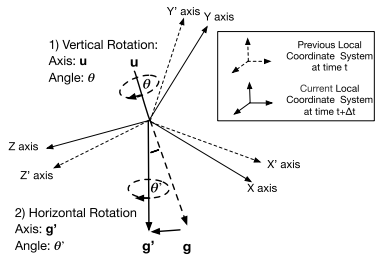

Fig. 12. Estimate the rotation matrix $\mathbf{A}_{t,t+\delta t}$.

those acceleration measurements only from the *positive time intervals* to extract the accumulated positive magnitudes of the consistent acceleration $\mathbf{f}_c(t)$. According to the formulation in Eq.(1), for the accumulated acceleration measurements, the accumulated positive magnitudes of $\mathbf{f}_c(t)$ dominates the result than the accumulated magnitudes of the inconsistent acceleration $\mathbf{f}'_i(t)$, which is very close to 0. In this way, we are able to further estimate the direction of $\mathbf{f}_c(t)$ in its local coordinate, according to its positive magnitudes in different axes. Therefore, we can estimate the direction of $\mathbf{f}_c(t)$ according to Theorem 2.

Theorem 2: Let α_i, β_i and γ_i be the constant angles between the consistent acceleration $\mathbf{f}_c(t)$ and the x, y and z axes in the reference local coordinate, respectively. Let $f_c(t)$ be the magnitude of $\mathbf{f}_c(t)$, and $f_{i,x}(t)$, $f_{i,y}(t)$ and $f_{i,z}(t)$ be the acceleration measurements in the x, y, and z-axes from the accelerometer, respectively. The direction of $\mathbf{f}_c(t)$ can be represented by a unit vector $\langle \cos\alpha_i, \cos\beta_i, \cos\gamma_i \rangle$, where the value of $\cos\alpha_i, \cos\beta_i$, and $\cos\gamma_i$ can be estimated as follows:

$$\begin{cases} \cos\widehat{\alpha}_i = \dfrac{E[f_{i,x}(t)]}{E[f_c(t)]} \\ \cos\widehat{\beta}_i = \dfrac{E[f_{i,y}(t)]}{E[f_c(t)]} \\ \cos\widehat{\gamma}_i = \dfrac{E[f_{i,z}(t)]}{E[f_c(t)]}. \end{cases} \tag{8}$$

Proof: Without loss of generality, we prove the equation $\cos\widehat{\alpha}_i = \frac{E[f_{i,x}(t)]}{E[f_c(t)]}$. According to Eq.(1), for the x-axis, $f_{i,x}(t) = f_c(t)\cos\widehat{\alpha}_i + f'_{i,x}(t)$. After we obtain a sequence of $f_{i,x}(t)$ from the positive time intervals in a sufficiently large time window W_p, the sum of $f_{i,x}(t)$ in these positive time intervals, *i.e.*, $\sum_{t\in W_p} f_{i,x}(t)$, can be depicted as follows:

$$\sum_{t\in W_p} f_{i,x}(t) = \sum_{t\in W_p} [f_c(t)\cdot\cos\widehat{\alpha}_i] + \sum_{t\in W_p} f'_{i,x}(t).$$

According to Theorem 1, $\sum_{t\in W_p} f'_{i,x}(t) \approx 0$. Besides, since $f_c(t)$ is extracted from the positive time intervals, then $\sum_{t\in W_p}[f_c(t)\cdot\cos\widehat{\alpha}_i] \gg \sum_{t\in W_p} f'_{i,x}(t)$. Thus,

$$\sum_{t\in W_p} f_{i,x}(t) \approx \sum_{t\in W_p} [f_c(t)\cdot\cos\widehat{\alpha}_i].$$

Moreover, since $\cos\widehat{\alpha}_i$ is constant, then,

$$\cos\widehat{\alpha}_i \approx \frac{\sum_{t\in W_p} f_{i,x}(t)}{\sum_{t\in W_p} f_c(t)} \approx \frac{E[f_{i,x}(t)]}{E[f_c(t)]}.$$

Similarly, we can prove that $\cos\widehat{\beta}_i = \frac{E[f_{i,y}(t)]}{E[f_c(t)]}$ and $\cos\widehat{\gamma}_i = \frac{E[f_{i,z}(t)]}{E[f_c(t)]}$. □

According to Theorem 2, our solution of estimating the direction of $\mathbf{f}_c(t)$ is as follows: First, we select a sufficiently large time interval to obtain the corresponding PCA results, and identify the positive time intervals from the PCA results where the accelerations are greater than 0. Then, for each axis of the reference local coordinate, we compute the expected value of the acceleration measurements within the above positive time intervals. After that, we can compute the angles α_i, β_i and γ_i according to Eq. (8), and estimate the direction of $\mathbf{f}_c(t)$. As the value of $E[f_c(t)]$ is the same in all three formulations in Eq. (8), it is actually unnecessary to compute the value of $E[f_c(t)]$. As a matter of fact, according to the previous analysis, we have $\sqrt{E[f_{i,x}(t)]^2 + E[f_{i,y}(t)]^2 + E[f_{i,z}(t)]^2} \approx E[f_c(t)]$.

VII. Gyroscope Based Orientation Tracking

A. Rotation Based Modeling

Our solution is based on the observation that the extracted direction of gravity is stable in the global coordinate. This observation can be further leveraged to calibrate the rotation matrix $\widehat{\mathbf{A}}_{t,t+\delta t}$ derived from gyroscope based tracking. For device D_i, suppose that the gravity is denoted as a vector $\mathbf{g} = \langle g_x(t), g_y(t), g_z(t)\rangle$ in the local coordinate system $L_i(t)$ at time t. Then, after a period of tracking, the gravity could be denoted as a different vector $\mathbf{g'} = \langle g_x(t+\delta t), g_y(t+\delta t), g_z(t+\delta t)\rangle$ in the local coordinate system $L_i(t+\delta t)$ at time $t+\delta t$. The difference between $\mathbf{g}$ and $\mathbf{g'}$ is caused by the rotation of the body frame from time t to time $t+\delta t$, we denote the corresponding rotation matrix as $\mathbf{A}_{t,t+\delta t}$. Thus we have $\mathbf{g'} = \mathbf{A}_{t,t+\delta t}\mathbf{g}$. According to the above relationship, the rotation matrix $\mathbf{A}_{t,t+\delta t}$ can be computed as follows. As shown in Fig. 12, note that due to the rotation of the body frame, there may exist a non-zero angle θ between the vectors $\mathbf{g'}$ and $\mathbf{g}$, it can be calculated as: $\theta = \arccos(\frac{\mathbf{g}\cdot\mathbf{g'}}{\|\mathbf{g}\|\|\mathbf{g'}\|})$, where the $\cdot$ operation refers to the *inner product* of the two vectors. During the process of rotation, to align the vector $\mathbf{g}$ to the vector $\mathbf{g'}$, it is essential to rotate axis $\mathbf{u}$ by an angle θ. The rotation axis $\mathbf{u}$ is orthogonal to the plane where the vectors $\mathbf{g}$ and $\mathbf{g'}$ lies on. Then, the rotation axis $\mathbf{u}$ can be obtained by computing the cross product of $\mathbf{g}$ and $\mathbf{g'}$: $\mathbf{u} = \frac{\mathbf{g}\times\mathbf{g'}}{\|\mathbf{g}\times\mathbf{g'}\|}$. We call the above rotation as the *vertical rotation*. Therefore, according to the Rodrigues' rotation formula [28], we compute the corresponding rotation matrix R as:

$$\mathbf{R} = \mathbf{I} + (\sin\theta)\mathbf{U} + (1-\cos\theta)\mathbf{U}^2 \tag{9}$$

where $\mathbf{I}$ is a 3×3 unit matrix, and $\mathbf{U}$ denote the *cross-product matrix* for vector $\mathbf{u}$.

By now we have obtained the rotation matrix by rotating the body frame to align the previous gravity vector **g** to the current gravity vector **g'** in the vertical direction. However, there still exists another degree of freedom in the horizontal direction because the body frame can rotate about the current gravity vector **g'** by any angle θ' on the horizontal plane. Thus, we need to further compute the rotation matrix **R'** with the rotation angle θ' on the horizontal plane to accurately estimate the rotation matrix $\mathbf{A}_{t,t+\delta t}$. As the body frame is rotated around the current gravity vector **g'**, then the rotation axis can be defined by a unit vector **u'** by normalizing the gravity vector **g'**, *i.e.*, $\mathbf{u'} = \frac{\mathbf{g'}}{\|\mathbf{g'}\|}$. According to the Rodrigues' rotation formula, suppose the rotation angle in the horizontal plane is θ', we compute the corresponding rotation matrix $\mathbf{R'}(\theta')$ as follows:

$$\mathbf{R}'(\theta') = \mathbf{I} + (\sin\theta')\mathbf{U}' + (1-\cos\theta')\mathbf{U}'^2 \tag{10}$$

where $\mathbf{I}$ is a 3×3 unit matrix, and $\mathbf{U}'$ denote the *cross-product matrix* for the vector **u'**. We call the above rotation as the *horizontal rotation*. Therefore, the rotation matrix $\widehat{\mathbf{A}}_{t,t+\delta t}$ can be estimated as follows:

$$\mathbf{A}_{t,t+\delta t}(\theta') = \mathbf{R}\mathbf{R}'(\theta') \tag{11}$$

Fig. 12 illustrates the two rotations for estimating the rotation matrix $\widehat{\mathbf{A}}_{t,t+\delta t}$.

B. Calibration With MMSE Estimator

According to the observations in previous work [6], [7] and the analysis in Section 4, we know that after a long period of tracking, there could be a fairly large error for the estimator $\widehat{\mathbf{A}}_{t,t+\delta t}$ of gyroscope tracking. Fortunately, we have already calculated a rotation matrix $\mathbf{A}_{t,t+\delta t}(\theta')$ from the rotation-based model. As the gravity direction can be accurately extracted through low pass filters such as the Butterworth filter, we actually obtain an accurate formulation of the rotation matrix $\mathbf{A}_{t,t+\delta t}$ with an unknown variable θ'. Thus, to estimate the rotation angle θ' according to the estimator $\widehat{\mathbf{A}}_{t,t+\delta t}$ from the gyroscope tracking, we leverage the Minimal Mean Squared Error (MMSE) estimator. We define the estimation error matrix as $E = \widehat{\mathbf{A}}_{t,t+\delta t} - \mathbf{A}_{t,t+\delta t}$, where the mean squared error (MSE) e is:

$$e(\theta') = \sum_{i=1}^{3}\sum_{j=1}^{3}(E_{i,j}(\theta'))^2 = \sum_{i=1}^{3}\sum_{j=1}^{3}(\widehat{\mathbf{A}}_{i,j} - \mathbf{A}_{i,j}(\theta'))^2$$

We then compute the optimal value of θ' that achieves the minimal mean squared error for the estimator $\widehat{\mathbf{A}}_{t,t+\delta t}$:

$$\theta'^* = \text{argmin}_{\theta'} e(\theta') \tag{12}$$

Thus, after computing the optimal value θ'^*, we use the rotation matrix $\mathbf{A}_{t,t+\delta t}(\theta'^*)$ as the calibrated estimator for the rotation matrix $\mathbf{A}_{t,t+\delta t}$.

VIII. Discussions and Limitations

A. Discussions

Timing for Space Synchronization: During the process of human motions, we need to find the time that all devices experience a consistent acceleration. We address this issue based on the observation that if multiple devices are subject to a consistent accelerations, then all the accelerometers of the devices should experience similar accelerations at a coarse level [29], [30], as the accelerations due to human motions are likely to dominate the accelerations caused by other intra-body motions. Thus, for each pair of devices, we compute the correlation of the measured accelerations at 1-10 Hz frequencies, which are the frequency range of human motions. We use a Support Vector Machine based classifier to determine whether all devices are subject to a consistent acceleration according to their pair-wise correlations.

Direction Change of Consistent Acceleration: During the process of human motions, the consistent acceleration could be also changing by the human subject over time. The change of the direction could be performed intentionally when the human subject is turning around or unintentionally when the human subject is slightly off the straight path. In such situations, it is essential to synchronize the global frames derived from the consistent acceleration with different directions; otherwise, the global coordinates cannot be consistent with each other. We address this issue as follows: Suppose that all devices are subject to two different forwarding accelerations with different directions at time t_{k-1} and t_k, respectively. After PCA, for each device, we obtain the two forwarding accelerations based on the reference local coordinate, *i.e.*, $\mathbf{f}_c(t_{k-1})$ and $\mathbf{f}_c(t_k)$, respectively. We calculate the angle deviation between $\mathbf{f}_c(t_{k-1})$ and $\mathbf{f}_c(t_k)$ on the horizontal plane as η_i for each device. After that, we compute the average value $\bar{\eta}$ from all m devices to mitigate the variances in estimating the angle deviation. Then, we use the angle deviation $\bar{\eta}$ as the direction change of the consistent acceleration to further calibrate the rotation matrix for space synchronization.

B. Limitations

Limitation to the Potential Application Scenarios: MOSS uses an estimator to derive a consistent direction on the horizontal plane, such as the moving direction. Combined with the gravity direction, MOSS build synchronized coordinates among different mobile devices. Hence, a consistent acceleration on the horizontal plane for multiple devices is essential for space synchronization. This requirement may not be satisfied for all applications. In some applications, e.g., when a human subject is jumping up and down with multiple devices, the consistent acceleration only exist on the vertical plane, which does not help to build synchronized coordinates among these devices. Besides, even if there exists a consistent acceleration for multiple devices on the horizontal plane, when the consistent acceleration changes from time to time in a frequent manner, the time window to collect the samplings of the acceleration might be too small, such that the consistent acceleration cannot be effectively extracted from the limited time window. Thus, the application scope of MOSS does have some limitations in the property of consistent acceleration.

Vulnerability to Sudden Activities: MOSS achieves good performance when the human subject is performing regular free activities, such as walking, jumping, and running, in which the arm's or hand's movements in these activities are relatively

simple and regular. However, in more general activities, e.g., the activities for VR applications, in which the motions can lead to sudden, rapid and irregular acceleration and orientation changes, MOSS may not achieve ideal performance for the following reasons: 1) In sudden activities, the inconsistent accelerations can be comparable to the consistent acceleration in the magnitude of the movement, such that the consistent acceleration cannot be effectively extracted. Besides, as aforementioned, the time window for the consistent acceleration can be too small, this further increases the difficulty to extract the consistent acceleration. 2) Sudden activity may lead to large errors in the inertial measurements including the accelerometer measurements and gyroscope measurements. The errors in the accelerometer measurements further lead to difficulty in *achieving* space synchronization, whereas the errors in the gyroscope measurements further lead to difficulty in *maintaining* space synchronization. Therefore, MOSS is more or less vulnerable to the sudden activities due to the above reasons.

IX. Performance Evaluation

A. Implementation and Setup

Hardware: We implemented MOSS on 1 smart glasses (Google Glass 2) and 5 smart phones (SAMSUNG Galaxy S5). They were placed on a human subject as shown in Fig. 2. These devices were connected to an Android smartphone (SAMSUNG Galaxy S5) via the Bluetooth 4.0 interface, i.e., S_2 in Fig. 2. The Android smartphone S_2 continuously collected the accelerometer and gyroscope measurements from these devices, and processed these measurements.

Setup: We let 5 volunteers move along three different straight paths in outdoor environment. They moved along the paths in three different modes: 1) *walk:* the human subject walked in normal speed (0.5$\sim$1 m/s) with small-amplitudes; 2) *run:* the human subject ran in fairly fast speed (2$\sim$3m/s) with large-amplitudes; 3) *jump:* the human subject jumped forward with large-amplitudes. For each path, we collected 20 traces for each moving mode. In each trace, we collected the inertial measurements from the accelerometers, gyroscopes, and magnetometers of all devices for a maximum time interval of 30 seconds. We collected a total of 120 traces of inertial measurements. To validate the performance against the ground truth, we extracted the magnetic direction and gravity direction from the inertial measurement, and used them to build an earth coordinate system as the reference coordinate system E.

Metrics: We used two metrics to evaluate MOSS: (1) *Angle Accuracy*: the angle deviation between the estimated forwarding direction and the ground truth, (2) *Coordinate Accuracy*: the correlations between the measurements from the synchronized coordinate and ground truth.

B. Forwarding Direction Estimation

We compared our solution with two heuristic solutions using Kalman filter as baseline solutions, *i.e.*,

1) *MeanAcc:* it uses Kalman filter [31] to filter the inertial readings first, and then estimates the forwarding direction by averaging the acceleration in three axes of the *body frame* within a time window, respectively. Take the acceleration in x-axis as an example, we use $x_{k-1|k-1}$ to denote the estimated acceleration at time t_{k-1}. Then, we use Kalman filter to estimate the true acceleration $x_{k|k}$ at time t_k, while combining the last estimated acceleration $x_{k-1|k-1}$ at time t_{k-1} and the measurement z_k from the accelerometer at time t_k. Kalman filter is a recursive estimator, which contains a prediction phase and an update phase in each recursive process.

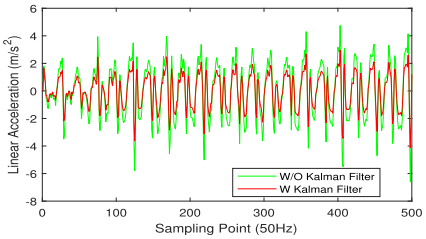

Fig. 13. Inertial readings with/without Kalman filter.

In the *prediction phase*, we use $x_{k-1|k-1}$ to predict the next acceleration as $x_{k|k-1}$, i.e., $x_{k|k-1} = x_{k-1|k-1}$. The estimate covariance $P_{k|k-1} = P_{k-1|k-1} + Q$, where $P_{k-1|k-1}$ means the estimate covariance in the last update phase, while Q means the covariance of the process noise in the prediction phase. Here, the process noise is assumed as Gaussian white noise $N(\mu_Q, Q)(Q = 1.0004$ in our implementation).

In the *update phase*, we combine the predicted acceleration $x_{k|k-1}$ and the measurement z_k to update the estimate of the acceleration $x_{k|k}$ at time t_k, i.e., $x_{k|k} = x_{k|k-1} + K_k(z_k - x_{k|k-1})$. Here, K_k means the Kalman gain at time t_k, and it can be calculated as follows: $K_k = P_{k|k-1}(P_{k|k-1} + R)^{-1}$, where R means the covariance of the measurement noise in the update phase, and the measurement noise is assumed as Gaussian white noise $N(\mu_R, R)$ ($R = 0.95976$ in our implementation). In the update phase, the estimate covariance $P_{k|k} = (1 - K_k)P_{k|k-1}$. Therefore, the optimal estimation of acceleration in x-axis at time t_k is $x_{k|k}$. Similarly, we can obtain the optimal estimation of the acceleration in y-axis, and z-axis at time t_k as $y_{k|k}$ and $z_{k|k}$, respectively. After that, we average the values of $x_{k|k}$, $y_{k|k}$, $z_{k|k}$ within a time window, respectively, to infer the forwarding direction. The solution is effective when the body frames of the devices do not change too much during the moving process.

2) *RefMeanAcc:* it estimates the forwarding direction by averaging the acceleration measurements within a time window respectively in three axes of the *reference local coordinate*. The main difference between *MeanAcc* and *RefMeanAcc* is that *RefMeanAcc* transforms all the acceleration from the *body frame* to the *reference local coordinate*. After that, *RefMeanAcc* calculates the acceleration in each axis based on Kalman filter [31] in the same way described in *MeanAcc*. The solution is effective even when the body frames of the devices keep changing, using the gyroscope tracking.

Experimental results show that Kalman filter can effectively remove the outliers or mitigate the jitters of the raw inertial readings. Fig. 13 shows the corresponding inertial readings with or without the Kalman filter. Note that in comparison to the raw inertial measurement, the inertial readings after the Kalman filter are more smooth and have less jitters. It implies that, for the situations where the human motions lead

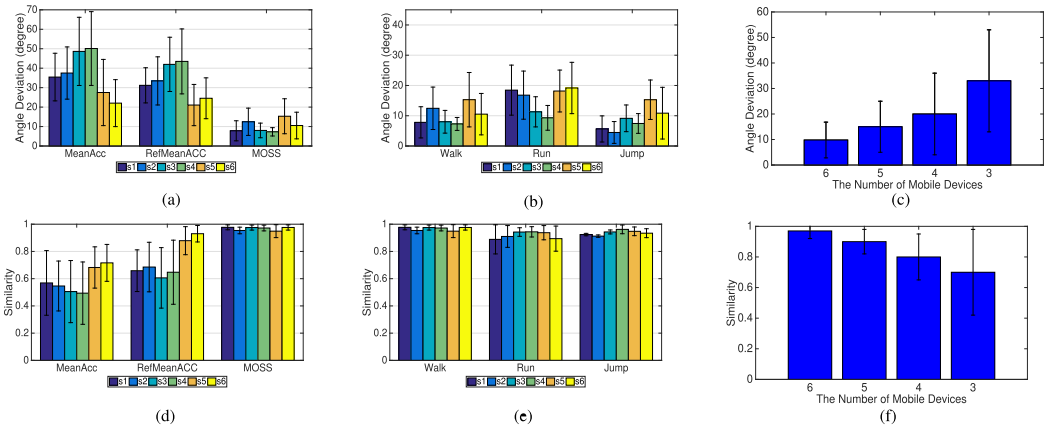

Fig. 14. Evaluate the accuracy of consistent forwarding direction estimation. (a) Angle accuracy for different forwarding direction estimators. (b) Angle accuracy for different moving modes. (c) Angle accuracy with different number of devices. (d) Coordinate accuracy for different forwarding direction estimators. (e) Coordinate accuracy for different moving modes. (f) Coordinate accuracy with different number of devices.

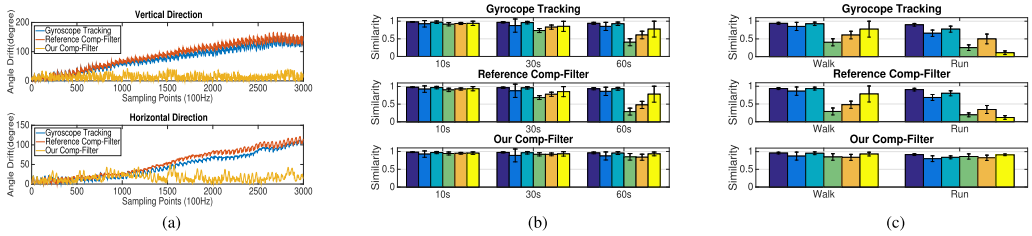

Fig. 15. Evaluate the accuracy of gyroscope-based orientation tracking. (a) Error accumulation over time for different solutions. (b) Coordinate accuracy for orientation tracking after different time intervals. (c) Coordinate accuracy for orientation tracking in different moving modes.

to sudden, rapid and irregular acceleration and orientation changes, the Kalman filter-based solution can effectively filter the corresponding inertial readings such that the performance cannot be degraded too much.

Experimental results show that MOSS achieves average angle accuracy of 9.8° *for all devices in different moving modes and with different time windows.* We first evaluated MOSS when the human subject is walking. Fig. 14(a) plots the angle deviation between the estimated forwarding direction and the ground truth, where we show the mean and standard deviation for all six devices. For MOSS, the average angle deviation in six devices are all less than 15° while the standard deviations are usually less than 9°. For both MeanACC and RefMeanACC, the average angle deviations are much greater than MOSS, besides, they all have much greater variances than MOSS. We further evaluated the average angle deviation respectively in walk, run, and jump, as shown in Fig. 14(b). We observed that MOSS achieves fairly good performance in angle accuracy for all three modes, which implies that MOSS is not very sensitive to the exact moving mode. Specifically, MOSS achieves best performance in the jump mode, as it generates larger consistent forwarding accelerations to assist space synchronization. The performance in the run mode degrades to some extent, as it generates larger inconsistent accelerations due to larger movements of the limbs.

Experimental results show that MOSS achieved average coordinate accuracy of 97% for all devices in different moving modes and with different time windows. We first evaluated the performance when the human subject is walking. Fig. 14(d) plots the correlations of measurements from the synchronized coordinate and ground truth. For MOSS, the average correlations from six devices are all greater than 95%. For MeanACC, most of the similarities are less than 60%, the similarity in S_4 is even as low as 49%. For RefMeanACC, the performance is increased to some extent, however, the average similarity is only 73%. We further evaluated the correlations of measurements in different moving modes as shown in Fig. 14(e). MOSS achieves good performance in measurement correlations for all three modes.

Experimental results show that, when the number of devices is varied from 3∼6, MOSS achieved fairly good performance in average angle accuracy and average coordinate accuracy. We vary the number of devices from 3 to 6, and evaluate the angle accuracy and coordinate accuracy, respectively. As shown in Fig. 14(c) and Fig. 14(f), it is found that, when the number of devices is decreased from 6 to 3, both the angle accuracy and coordinate accuracy is decreased accordingly, e.g., when the number of devices is decreased from 6 to 3, the average angle deviation is increased from 9.8° to 33° and the average similarity is is decreased from to 97% to 70%. This is caused by the reduced number of streams in the PCA process. Nevertheless, it still achieves fairly good performance on the whole.

C. Gyroscope-Based Orientation Tracking

We implemented the following solutions for performance comparison: 1) *Gyroscope Tracking:* the orientation tracking scheme purely based on the gyroscope measurements [12]. 2) *Reference Complementary Filter:* a common complementary filter combining the accelerometer and gyroscope data

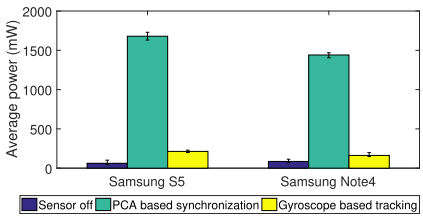

Fig. 16. The average power of different working modes.

to track the orientation [32]. 3) *Complementary Filter:* our solution of the complementary filter designed in Section 7.

Experimental results show that MOSS achieves average angle accuracy of 19° *in orientation tracking after 30 seconds.* Specifically, MOSS can effectively control the error accumulations for gyroscope based tracking in different moving modes and with different time intervals. To evaluate the error accumulation over time for different solutions, we evaluated the angle deviation of the gravity and magnetic direction, respectively, in a reference coordinate so as to measure the error accumulations in the vertical and horizontal directions, respectively. Fig. 15(a) plots the error accumulation in vertical and horizontal directions. Without loss of generality, we selected the measurements from the device S_4 as an example. We observed that in both directions, the errors of both the *gyroscope tracking* and the *reference complementary filter* keep increasing over time, whereas the error of our *complementary filter* does not accumulate over time. After 30 seconds, the errors of the former two solutions are over 110°, whereas the error of MOSS is no greater than 20°.

Experimental results show that MOSS achieves average coordinate accuracy of 85% in orientation tracking after 30 seconds. Specifically, MOSS achieves a high level of measurement correlations for gyroscope based tracking in different moving modes and with different time intervals. We evaluated the measurement correlations from the synchronized coordinate and ground truth after different time intervals in Fig. 15(b). As the time interval increases, we observed that the correlations of both gyroscope tracking and reference complementary filter keep decreasing, whereas the correlation of our solution always maintains at a high level. We further evaluated the measurement correlations in different moving modes in Fig. 15(c). For the run mode, the correlations of both gyroscope tracking and reference complementary filter are greatly reduced in comparison with the walk mode, which is due to the error accumulations caused by the large angular velocities and linear accelerations. Nevertheless, the average correlation of MOSS maintains to be 85% and 81%, respectively, in both walk and run mode.

D. Energy Consumption

Experimental results show that MOSS achieves average power of 1440∼1650mW in PCA-based synchronization and 162∼213mW in gyroscope-based tracking. Specifically, we use the Monsoon power monitor [33] to evaluate the power of PCA-based synchronization and gyroscope-based tracking, respectively, in the Samsung S5 platform and Samsung Note 4 platform. For each platform, we respectively evaluate the power of three processing modes, i.e., 1) *Sensor off*: all the sensors including the screens are turned off; 2) *PCA-based synchronization*: PCA is used to achieve space synchronization with inertial sensors turned on; 3) *Gyroscope-based tracking*: gyroscope-based tracking is used to maintain space synchronization with inertial sensors turned on. As shown in Fig.16, it is found that the PCA-based synchronization has average power of 1440∼1650mW, which is much larger than the power of the other two modes. However, since the PCA-based synchronization is only used to achieve space synchronization from time to time, it often occupies a small portion of the overall duration, e.g., 5%, the gyroscope-based tracking is used to maintain space synchronization in the rest of the overall duration, the energy consumption of PCA-based synchronization can be effectively amortized by the gyroscope-based tracking for energy efficiency.

X. Case Study: Space Synchronization via Free Activities

We performed space synchronization for multiple devices under a more real scenario, *i.e.*, the human subject carried six mobile devices in different parts of his/her body, and moved freely in the outdoor environment. Similar to the setup in Section 9.2, we let the volunteers move along different straight paths in outdoor environment. The only difference is that the human motion can be a combination of walk, run, and jump in any arbitrary approach. We used the consistent forwarding acceleration to *achieve* space synchronization when the human subject was moving forward. Moreover, during the moving process, the human subject could stop moving forward and take a break, while his/her limbs keep moving. We used the gyroscope tracking to *maintain* space synchronization when the human subject stopped moving forward. We collected a total of 30 traces from 5 volunteers for performance evaluation.

A. Space Synchronization Accuracy

Without loss of generality, we selected an example moving trace and target one of the six devices, *i.e.*, S_4, and continuously monitored the angle/coordinate accuracy of our MOSS scheme. The sampling time window was set to 3s. Fig. 17 shows the time intervals of the specified movements and the corresponding experiment result. For the angle accuracy, we observed that the angle deviation is continuously changing over time. During the time interval of walk, run, and jump, the angle deviation varies around the average value of 9°. During the time interval of rest, the angle deviation slightly increases along with time, due to the loss of the consistent forwarding acceleration. Nevertheless, the angle deviations are all less than 18°. For the coordinate accuracy, we observed that the similarity is also changing over time, nevertheless, they are all greater than 81%.

We then evaluated the performance of the consistent forwarding direction estimation (CFDE) and the gyroscope-based orientation tracking (GOT), respectively, in a statistical approach. Fig. 18 shows the experiment results during the compound moving process. For the performance of CFDE, as shown in Fig. 18(a), the angle accuracy of all devices are less than 17°, while the average accuracy is 12°, even if the moving process is mixed with different kinds of movements. In Fig. 18(b), the coordinate accuracy of all devices are greater

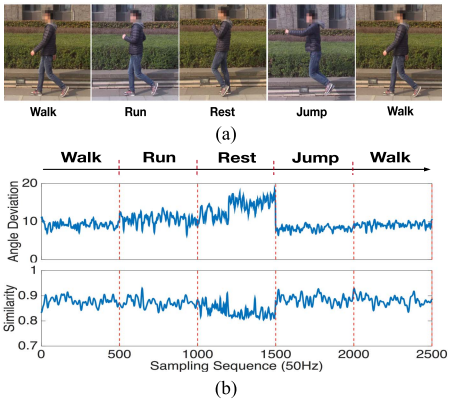

Fig. 17. Experiment results. (a) An example process of human movement. (b) The variation of angle/coordinate accuracy.

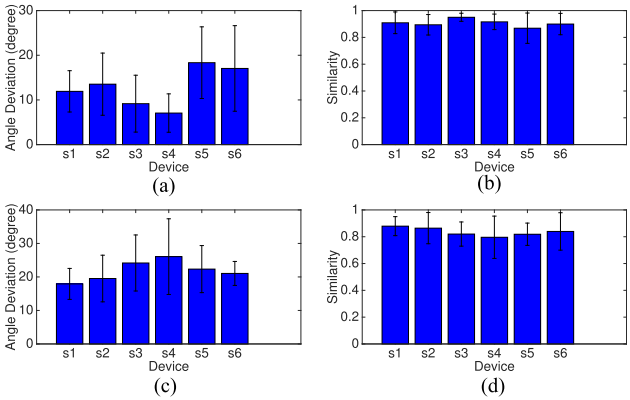

Fig. 18. Accuracy evaluation. (a) Angle accuracy of CFDE. (b) Coordinate accuracy of CFDE. (c) Angle accuracy of GOT. (d) Coordinate accuracy of GOT.

than 87%, while the average coordinate accuracy is 91%. For the performance of GOT, as the human subject stops moving forward, we evaluated the accuracy after a time interval of 30 seconds. As shown in Fig. 18(c), the angle accuracies of all devices are less than 26°, while the average accuracy is 21°, even if the time interval is as long as 30s. In Fig. 18(d), the coordinate accuracies of all devices are greater than 80%, while the average coordinate accuracy is 84%.

B. Activity Recognition Accuracy

Based on the synchronized coordinates, we further evaluate the performance in activity recognition, by using the methods of Dynamic Time Warping (DTW) and Random Forest (RF). Specifically, we let 10 volunteers perform 10 categories of activities, including Dumbbell Triceps Extension (DTE), Dumbbell Lateral Raise (DLR), Upright Barbell Row (UBR), Cable Crossover (CC), Butterfly (BF), Dumbbell Flies (DF), Rope Skipping (RS), Dumbbell Curl (DC), Ping-pong Swing (PS), and Badminton Swing (BS). In order to evaluate the impact on the recognition accuracy from the space synchronization, we plot the confusion matrix of activity recognition, respectively, based on Compass synchronized coordinates and MOSS synchronized coordinates. Fig. 19 shows the experiment results. Note that in regard to the DTW method, the average recognition accuracy is 84.6% for the Compass synchronized coordinate, whereas

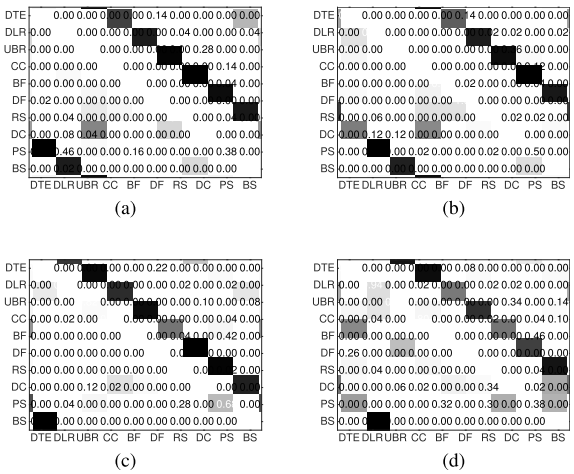

Fig. 19. Activity recognition accuracy. (a) DTW-based Recognition based on Compass sychronization. (b) DTW-based Recognition based on MOSS sychronization. (c) RF-based Recognition based on Compass sychronization. (d) RF-based Recognition based on MOSS sychronization.

the average recognition accuracy is 84.2% for the MOSS synchronized coordinate. In regard to the Random Forest method, the average recognition accuracy is 85.6% for the Compass synchronized coordinate, whereas the average recognition accuracy is 73.2% for the MOSS synchronized coordinate. This implies that the recognition performance is not dramatically degraded based on MOSS synchronization, since MOSS achieves fairly good performance in space synchronization.

XI. Conclusion

We made three key contributions in this paper. First, we investigate the problem of space synchronization for mobile devices. Second, we propose the MOSS scheme to achieve space synchronization among multiple mobile devices. In particular, we propose a consistent direction estimator to achieve space synchronization, and a gyroscope based orientation tracker to maintain space synchronization. Third, we implemented MOSS on COTS mobile devices, and the experiment results show that MOSS achieves an average angle accuracy of 9.8° and an average coordinate accuracy of 97%.

References

[1] S. Shen, H. Wang, and R. R. Choudhury, "I am a smartwatch and i can track my user's arm," in *Proc. MobiSys*, 2016, pp. 85–96.
[2] L. Zhang *et al.*, "It starts with iGaze: Visual attention driven networking with smart glasses," in *Proc. MobiCom*, 2014, pp. 91–102.
[3] C. Karatas *et al.*, "Leveraging wearables for steering and driver tracking," in *Proc. IEEE INFOCOM*, Apr. 2016, pp. 1–9.
[4] J. Yu *et al.*, "SenSpeed: Sensing driving conditions to estimate vehicle speed in urban environments," *IEEE Trans. Mobile Comput.*, vol. 15, no. 1, pp. 202–216, Jan. 2016.
[5] Z. Sun *et al.*, "Polaris: Getting accurate indoor orientations for mobile devices using ubiquitous visual patterns on ceilings," in *Proc. ACM HotMobile*, 2012, pp. 14:1–14:6.
[6] P. Zhou, M. Li, and G. Shen, "Use it free: Instantly knowing your phone attitude," in *Proc. MobiCom*, 2014, pp. 605–616.
[7] S. Poddar, V. Kumar, and A. Kumar, "A comprehensive overview of inertial sensor calibration techniques," *J. Dyn. Syst., Meas. Control*, vol. 139, no. 1, p. 011006, 2016.
[8] H. Fourati, "Heterogeneous data fusion algorithm for pedestrian navigation via foot-mounted inertial measurement unit and complementary filter," *IEEE Trans. Instrum. Meas.*, vol. 64, no. 1, pp. 221–229, Jan. 2015.

[9] B. Barshan and H. Durrant-Whyte, "Inertial navigation systems for mobile robots," *IEEE Trans. Robot. Automat.*, vol. 11, no. 3, pp. 328–342, Jun. 1995.
[10] H.-J. Lee and S. Jung, "Gyro sensor drift compensation by Kalman filter to control a mobile inverted pendulum robot system," in *Proc. IEEE ICIT*, Feb. 2009, pp. 1–6.
[11] J. Marins, X. Yun, E. Bachmann, R. Mcghee, and M. Zyda, "An extended Kalman filter for quaternion-based orientation estimation using MARG sensors," in *Proc. IEEE/RSJ IROS*, Oct./Nov. 2001, pp. 2003–2011.
[12] J. O. Woodman, "An introduction to inertial navigation," Dept. Comput. Lab., Univ. Cambridge, Cambridge, U.K., Tech. Rep. UCAM-CL-TR696, 2007.
[13] S. Madgwick, A. J. L. Harrison, and R. Vaidyanathan, "Estimation of IMU and MARG orientation using a gradient descent algorithm," in *Proc. IEEE ICORR*, Jun./Jul. 2011, pp. 1–7.
[14] M. Gowda *et al.*, "Bringing IoT to sports analytics," in *Proc. 14th USENIX Symp. Netw. Syst. Design Implement. (NSDI)*, 2017, pp. 499–513.
[15] J. Metge, R. Mégret, A. Giremus, Y. Berthoumieu, and T. Décamps, "Calibration of an inertial-magnetic measurement unit without external equipment, in the presence of dynamic magnetic disturbances," *Meas. Sci. Technol.*, vol. 25, no. 12, p. 125106, 2014.
[16] A. Baak, T. Helten, M. Müller, G. Pons-Moll, B. Rosenhahn, and H. Seidel, "Analyzing and evaluating markerless motion tracking using inertial sensors," in *Proc. 11th Eur. Conf. Trends Topics Comput. Vis. (ECCV)*, vol. 1, 2012, pp. 139–152.
[17] T. von Marcard, B. Rosenhahn, M. J. Black, and G. Pons-Moll, "Sparse inertial poser: Automatic 3D human pose estimation from sparse IMUs," in *Proc. EUROGRAPHICS*, 2017, pp. 499–513.
[18] S. Guha *et al.*, "AutoWitness: Locating and tracking stolen property while tolerating GPS and radio outages," in *Proc. ACM SenSys*, 2010, pp. 29–42.
[19] P. Mohan, V. N. Padmanabhan, and R. Ramjee, "Nericell: Using mobile smartphones for rich monitoring of road and traffic conditions," in *Proc. ACM SenSys*, 2008, pp. 357–358.
[20] N. Roy, H. Wang, and R. R. Choudhury, "I am a smartphone and I can tell my user's walking direction," in *Proc. MobiSys*, 2014, pp. 329–342.
[21] G. Shen, Z. Chen, P. Zhang, T. Moscibroda, and Y. Zhang, "Walkie-Markie: Indoor pathway mapping made easy," in *Proc. USENIX NSDI*, 2013, pp. 85–98.
[22] H. Wang *et al.*, "No need to war-drive: Unsupervised indoor localization," in *Proc. ACM MobiSys*, 2012, pp. 197–210.
[23] J. A. B. Link, P. Smith, N. Viol, and K. Wehrle, "FootPath: Accurate map-based indoor navigation using smartphones," in *Proc. IPIN*, 2011, pp. 1–8.
[24] X. Zhu, Q. Li, and G. Chen, "APT: Accurate outdoor pedestrian tracking with smartphones," in *Proc. IEEE INFOCOM*, Apr. 2013, pp. 2508–2516.
[25] M. Afzal, V. Renaudin, and G. Lachapelle, "Magneticfield based heading estimation for pedestrian navigation environments," in *Proc. IPIN*, 2011, pp. 1–10.
[26] S.-W. Lee, P. Jung, and S.-H. Song, "Hybrid indoor location tracking for pedestrian using a smartphone," in *Robot Intelligence Technology and Applications*. Berlin, Germany: Springer, 2013, pp. 431–440.
[27] S. Butterworth, "On the theory of filter amplifiers," *Wireless Engineer*, vol. 7, no. 6, pp. 536–541, 1930.
[28] O. Rodrigues, "Des lois géométriques qui régissent les déplacements d'un systéme solide dans l'espace, et de la variation des coordonnées provenant de ces déplacements considérés indépendamment des causes qui peuvent les produire," *J. Math. Pures Appl.*, vol. 5, pp. 380–440, 1840.
[29] J. Lester, B. Hannaford, and G. Borriello, "'Are you with me?'—Using accelerometers to determine if two devices are carried by the same person," in *Proc. Pervasive Comput. (Pervasive)*, 2004, pp. 33–50.
[30] C. T. Cornelius and D. F. Kotz, "Recognizing whether sensors are on the same body," *Pervasive Mobile Comput.*, vol. 8, no. 6, pp. 822–836, 2012.
[31] R. Faragher, "Understanding the basis of the Kalman filter via a simple and intuitive derivation," *IEEE Signal Process. Mag.*, vol. 29, no. 5, pp. 128–132, Sep. 2012.
[32] (2013). *Reading a IMU Without Kalman: The Complementary Filter*. [Online]. Available: http://www.pieter-jan.com/node/11
[33] Monsoon Solutions Inc. (2015). *Monsoon Power Monsoon Power Monitor*. [Online]. Available: https://www.msoon.com/LabEquipment/PowerMonitor

Lei Xie received the B.S. and Ph.D. degrees in computer science from Nanjing University, China, in 2004 and 2010, respectively. He is currently an Associate Professor with the Department of Computer Science and Technology, Nanjing University. He has published over 60 papers in the IEEE/ACM TRANSACTIONS ON NETWORKING, the IEEE TRANSACTIONS ON MOBILE COMPUTING, the IEEE TRANSACTIONS ON PARALLEL AND DISTRIBUTED SYSTEMS, *ACM Transactions on Sensor Networks*, ACM MobiCom, ACM UbiComp, ACM MobiHoc, IEEE INFOCOM, IEEE ICNP, and IEEE ICDCS.

Qingliang Cai received the B.S. degree in software engineering from Suzhou University, China, in 2014, and the M.S. degree from the Department of Computer Science and Technology, Nanjing University, in 2017. His research interests include wearable computing.

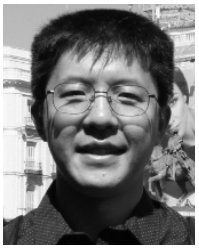

Alex X. Liu received the Ph.D. degree in computer science from The University of Texas at Austin in 2006. His research interests focus on networking and security. He received the IEEE & IFIP William C. Carter Award in 2004, the National Science Foundation CAREER Award in 2009, and the Michigan State University Withrow Distinguished Scholar Award in 2011. He received Best Paper Awards from ICNP-2012, SRDS-2012, and LISA-2010. He is an Associate Editor of the IEEE/ACM TRANSACTIONS ON NETWORKING, an Editor of the IEEE TRANSACTIONS ON DEPENDABLE AND SECURE COMPUTING, and an Area Editor of *Computer Communications*.

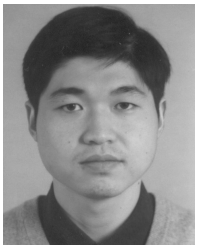

Wei Wang received the M.S. degree from the ESE Department, Nanjing University, in 2000, and the Ph.D. degree from the ECE Department, National University of Singapore, in 2008. He is currently an Associate Professor with the CS Department, Nanjing University. His research interests are in the area of wireless networks, including device-free sensing, cellular network measurements, and software defined radio systems.

Yafeng Yin received the B.E. degree in network engineering from the Nanjing University of Science and Technology in 2011, and the Ph.D. degree in computer science from Nanjing University, China, in 2017. She is currently an Assistant Professor with the Department of Computer Science and Technology, Nanjing University. Her research interests include human activity recognition, mobile sensing, and wearable computing.

Sanglu Lu received the B.S., M.S., and Ph.D. degrees in computer science from Nanjing University, China, in 1992, 1995, and 1997, respectively. She is currently a Professor with the Department of Computer Science and Technology, Nanjing University. Her research interests include distributed computing and pervasive computing.